# Supporting Information

# Effect of Chelators on the Pharmacokinetics of $^{99m}$Tc-Labeled Imaging Agents for the Prostate-Specific Membrane Antigen (PSMA)

Sangeeta Ray Banerjee*, Mrudula Pullambhatla, Catherine A. Foss, Alexander Falk, Youngjoo Byun, Sridhar Nimmagadda, Ronnie C. Mease, Martin G. Pomper*

Russell H. Morgan Department of Radiology and Radiological Sciences, Johns Hopkins Medical Institutions, Baltimore, MD 21231

**Corresponding Author:** Martin G. Pomper, M.D., Ph.D., Johns Hopkins Medical Institution, 1550 Orleans Street, 492 CRB II, Baltimore, MD 21287, 410-955-2789 (T443-817-0990 (F), mpomper@jhmi.edu

**Co-corresponding Author**: Sangeeta Ray Banerjee, Johns Hopkins Medical Institution, 1550 Orleans Street, 4M07 CRB II, Baltimore, MD 21287, Ph.D, 410-955-8697, sray9@jhmi.edu

# Table of Contents

# General Experimental Methods

Solvents and chemicals obtained from commercial sources were of analytical grade or better and used without further purification. S-trityl mercaptoacetic acid and Boc-L-propargylglycine were purchased from AnaSpec. All 9-fluorenylmethyloxycarbonyl (Fmoc) protected amino acids including the Fmoc-Lys(Boc)-Wang resin,1-Hydroxybenzotriazole monohydrate (HOBT) and 2-(1H-benzotriazole-1-yl)-1,1,3,3-tetramethyluronium hexafluorophosphate (HBTU) were purchased from Chem Impex International Inc. (Wooddale, IL). Hynic(Boc)-NHS ester was purchased from Solulink (San Diego, California). All experiments were performed in duplicate or triplicate to ensure reproducibility. Analytical thin-layer chromatography (TLC) was performed using Aldrich aluminum-backed 0.2 mm silica gel Z19, 329-1 plates and visualized by ultraviolet light (254 nm), $I_2$ and 1% ninhydrin in EtOH. Flash chromatography was performed using silica gel purchased from Bodman (Aston PA), MP SiliTech 32-63 D 60Å. $^1$H NMR spectra were recorded on a Bruker ultrashield$^{TM}$ 400 MHz spectrometer. Chemical shifts (δ) are reported in ppm downfield by reference to proton resonances resulting from incomplete deuteration of the NMR solvent. Low resolution ESI mass spectra were obtained on a Bruker Daltonics Esquire 3000 Plus spectrometer. High resolution mass spectra were obtained by the University of Notre Dame Mass Spectrometry & Proteomics Facility, Notre Dame, IN using ESI either by direct infusion on a Bruker micrOTOF-II or by LC elution *via* an ultra-high pressure Dionex RSLC with $C_{18}$ column coupled with a Bruker micrOTOF-Q II. High-performance liquid chromatographic purification of new compounds, **L8-L19,** were performed using a Phenomenex $C_{18}$ Luna 10 × 250 mm$^2$ 10 μm column on a Waters 600E Delta LC system with a Waters 486 tunable absorbance UV/Vis detector, both controlled by Empower software. HPLC purification of radiolabeled compounds were performed on a Varian Prostar System (Palo Alto, CA), equipped with a Varian Prostar 325 variable wavelength UV detector and a a Bioscan Flow-count in-line Radioactivity detector . The specific radioactivity was calculated as the

radioactivity eluting at the retention time of product during the preparative HPLC purification divided by the mass corresponding to the area under the curve of the UV absorption.

**Table S1**. Octanol/water partition coefficient ($P_{oct/water}$) and HPLC retention time ($R_t$) of selected compounds

| Compound | $P_{oct/water}$ | $R_t$ (min) |
|---|---|---|
| **$^{99m}$TcL1** | -2.03 | 26 (b) |
| **$^{99m}$ TcL8** | -2.37 | 27.9 (a) 22.2 min(c) |
| **$^{99m}$ TcL9** | -2.05 | 24 min (b) |
| **$^{99m}$ TcL10** | -2.07 | 37.6 (a) |
| **$^{99m}$ TcL11** | -2.38 | ~17 min (c ) |
| **$^{99m}$ TcL12** | -2.25 | ~20 min (c) |
| **$^{99m}$ TcL13** | -2.14 | 17.5 (d), 21.8 (c) |
| **$^{99m}$ TcL14** | -2.35 | 14.7 (c) |
| **$^{99m}$ TcL15** | -3.04 | 11.4 (c) |
| **$^{99m}$ TcL16** | N.D. | 17.67(c) |
| **$^{99m}$TcL17** | -2.96 | 15.2 (c) |
| **$^{99m}$ TcL18** | -2.94 | 12.9 (c) |
| **$^{99m}$ TcL19** | -3.05 | 11.4 (e) |

[a] HPLC method 1; [b] HPLC method 2; [c] HPLC method 3; [d] HPLC method 4; [e] HPLC method 5; N.D. (not determined)

## Spectral Data

$^{1}$H (top) and $^{13}$C NMR (bottom) spectra for [Re(CO)$_3$]**L8** in DMSO-*d6* at room temperature

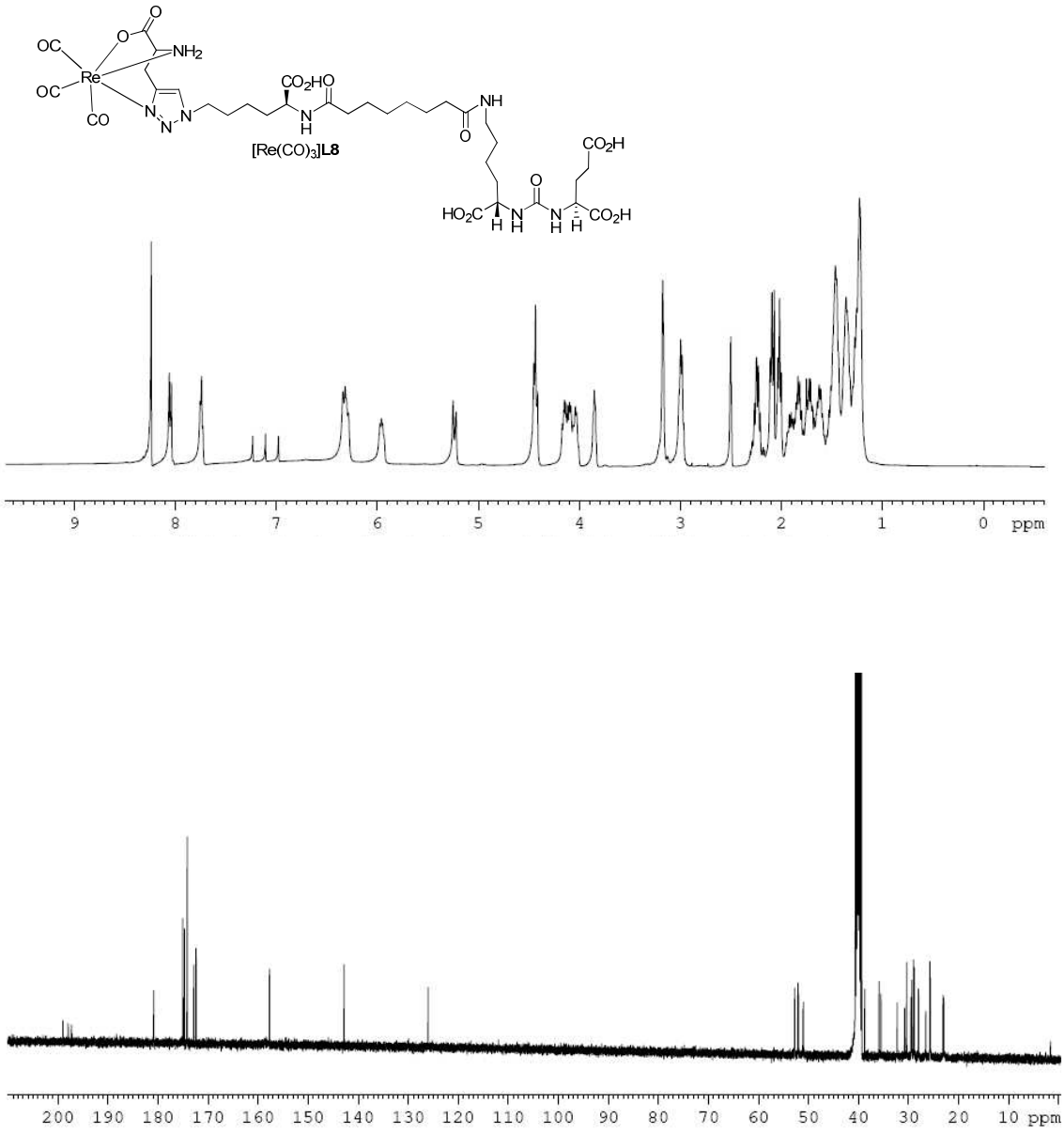

HPLC chromatograms of cold [Re]**L8**; uv peak at λ= 254 nm (top), peak at λ = 220 nM (bottom).

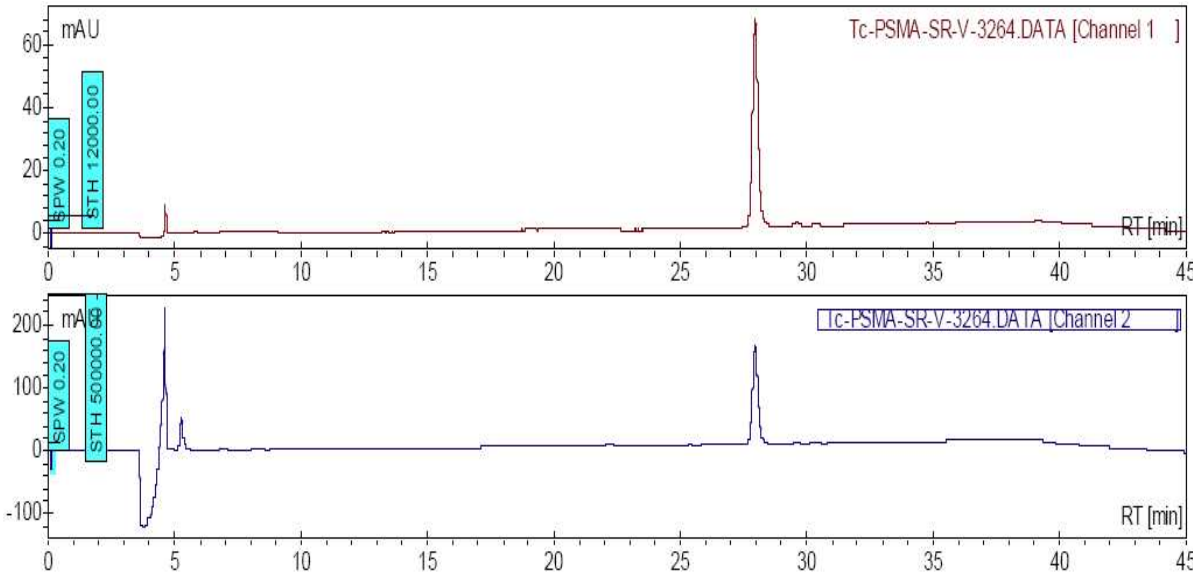


Standard curve (area of absorbance vs mass) and the detection limit of [Re]**L8**

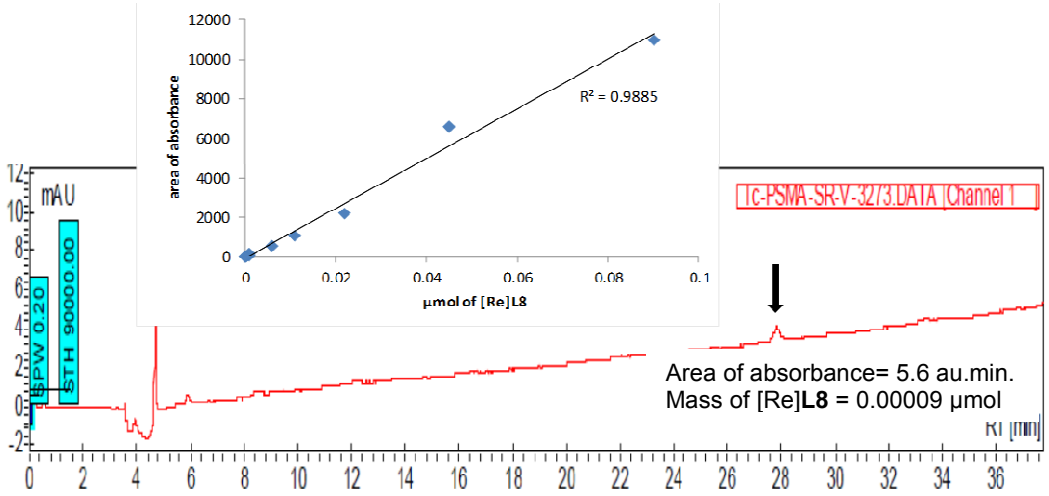

Preparative HPLC chromatograms for [$^{99m}$Tc]**L8**; radio-HPLC peak (top) uv peak at λ = 220 nM (bottom).

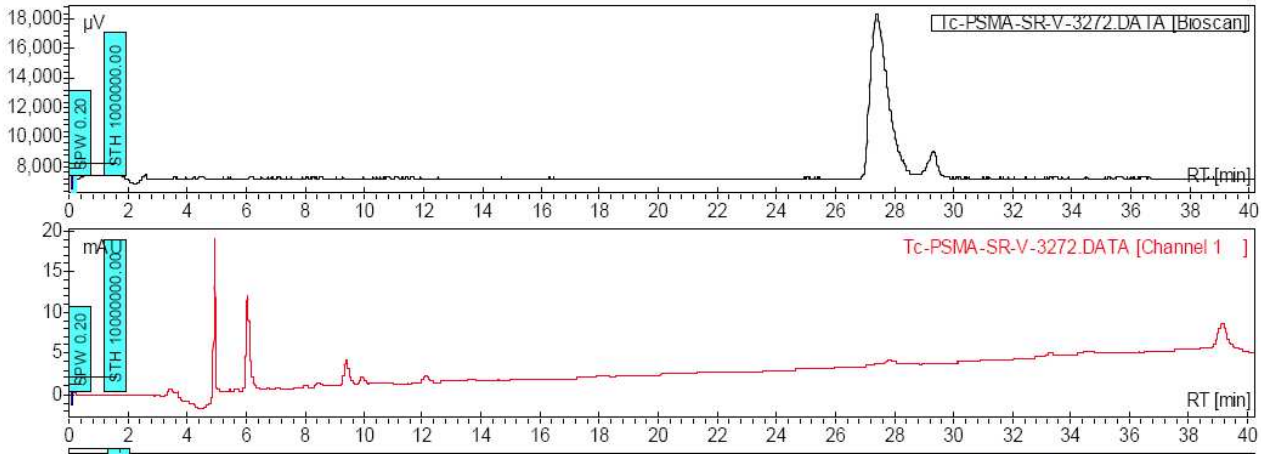


HPLC chromatograms for pure [$^{99m}$Tc]**L8**; a. radio-HPLC peak, uv peak at λ = 220 nM (bottom).

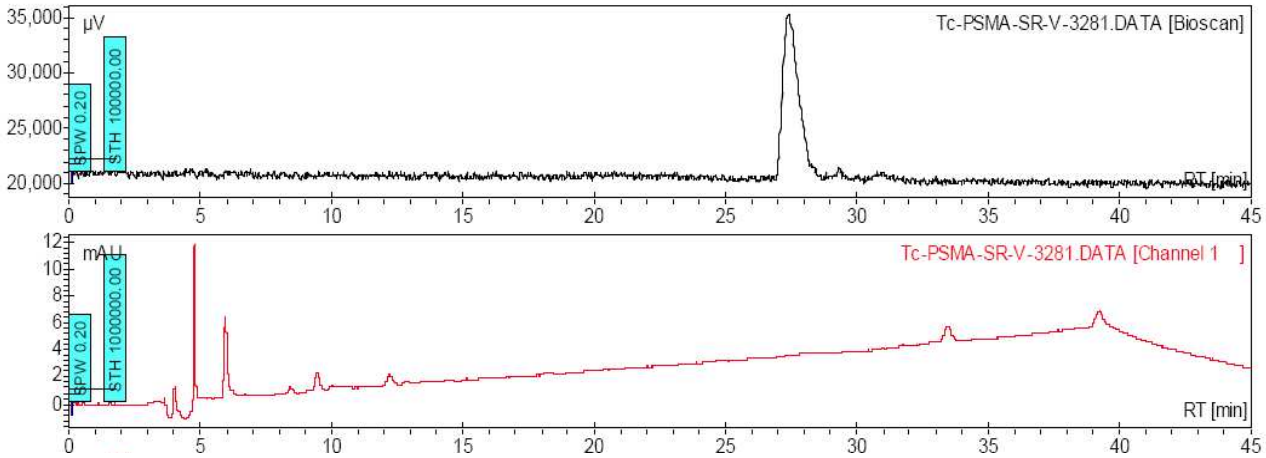

Stability study for [$^{99m}$Tc]**L8**. HPLC chromatograms for [$^{99m}$Tc]**L8** and [Re]**L8** (coinjection) after incubation of [$^{99m}$Tc]**L8** in 1X PBS solution at 25°C for 24 h; radio-HPLC peak of [$^{99m}$Tc]**L8** (top). UV peak at λ= 254 nm (middle) of [Re]**L8**, peak at λ = 220 nM of [Re]**L8** (bottom) (HPLC Method 1).

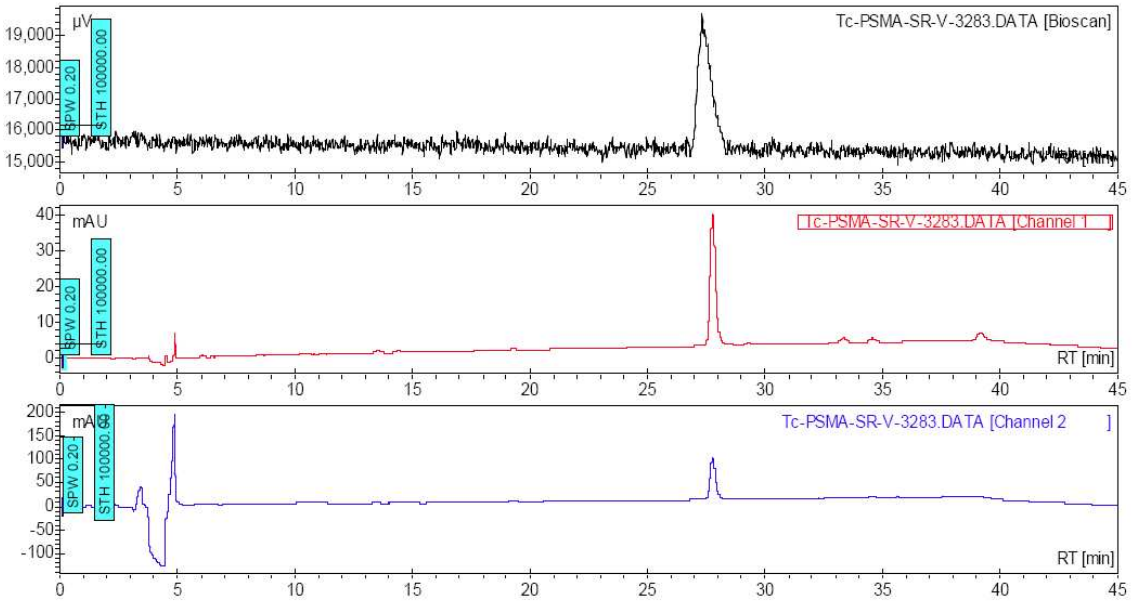


Preparative HPLC chromatograms for [$^{99m}TcO_4$]$^-$ in presence of $SnCl_2$ and tartrate ; radio-HPLC peak (top) uv peak at λ= 254nm (bottom) (HPLC Method 3).

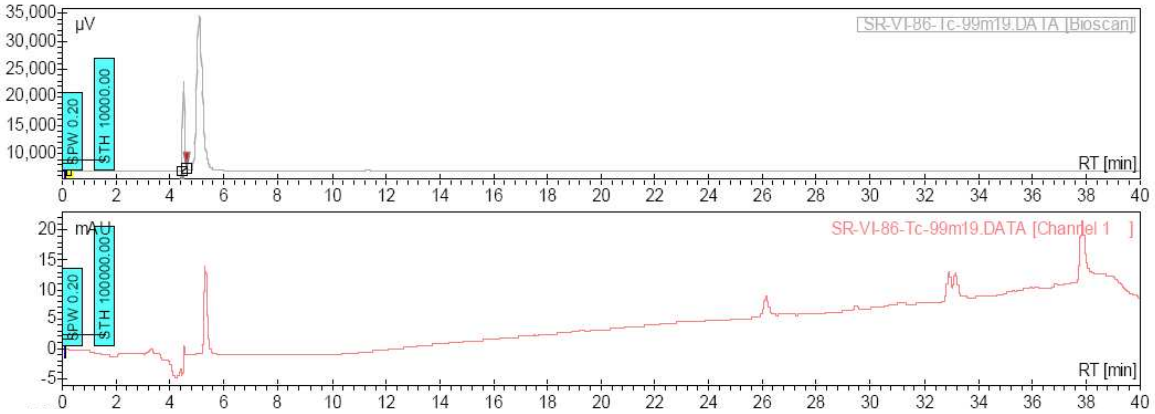

Preparative HPLC chromatograms for [$^{99m}$Tc]**L9**; radio-HPLC peak (top) uv peak at λ= 254nm (middle and bottom) (HPLC Method 2). The large uv peak at 9.5 min is unchelated **L9**.

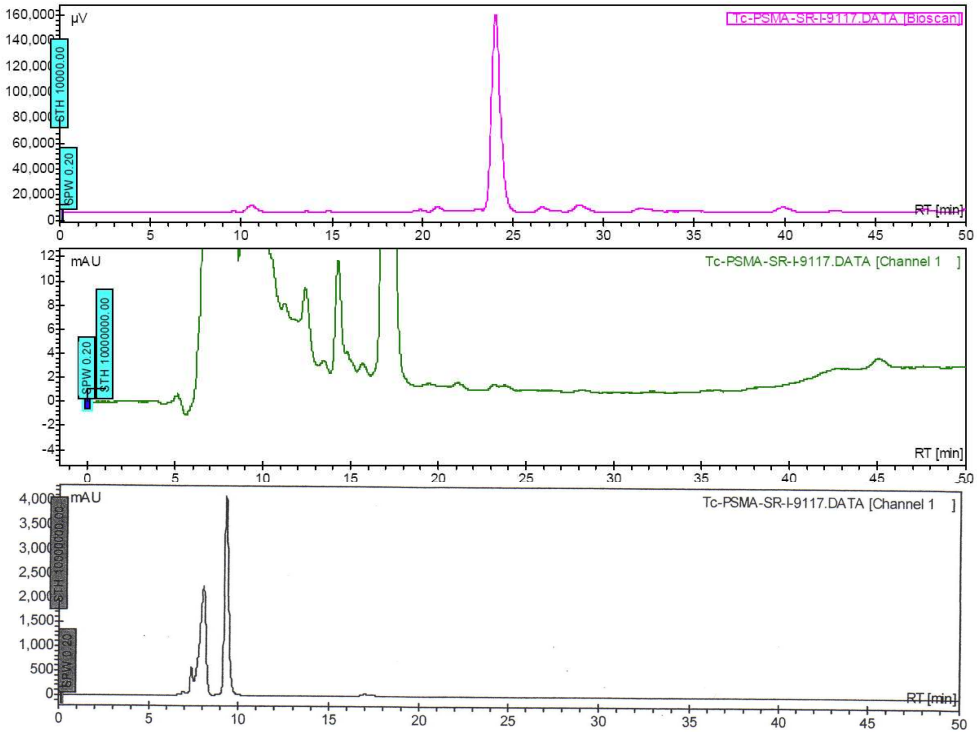


Preparative HPLC chromatograms for [$^{99m}$Tc]**L10**; radio-HPLC peak (top) uv peak at λ= 254nm (bottom) (HPLC Method 1). The uv peak at 10.5 min is unchelated **L10**

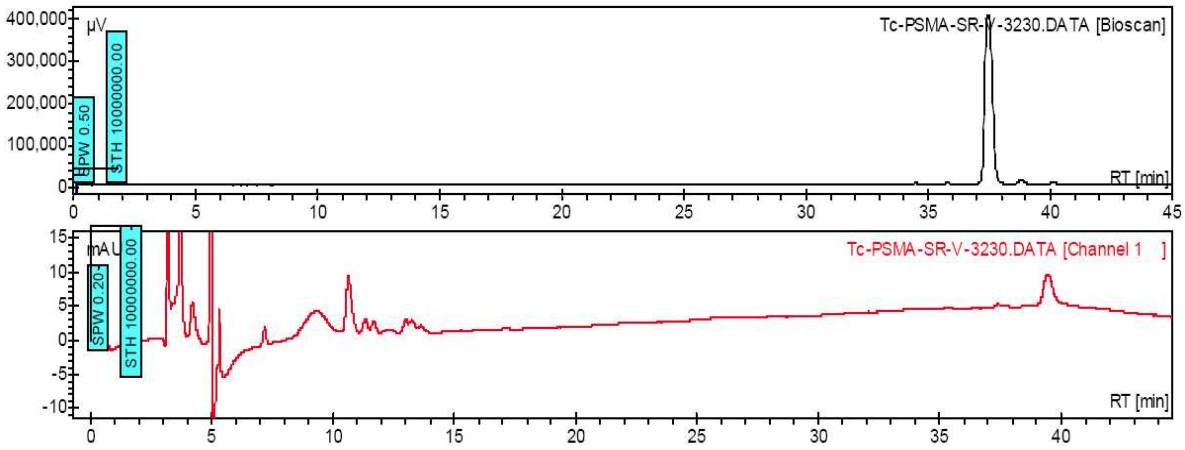

Preparative HPLC chromatograms for [$^{99m}$Tc]**L11**; radio-HPLC peak (top) uv peak at λ= 254nm (middle and bottom) (HPLC Method 3). The uv peak at 34 min is for the unchelated **L11** as shown in full scale in the bottom chromatogram.

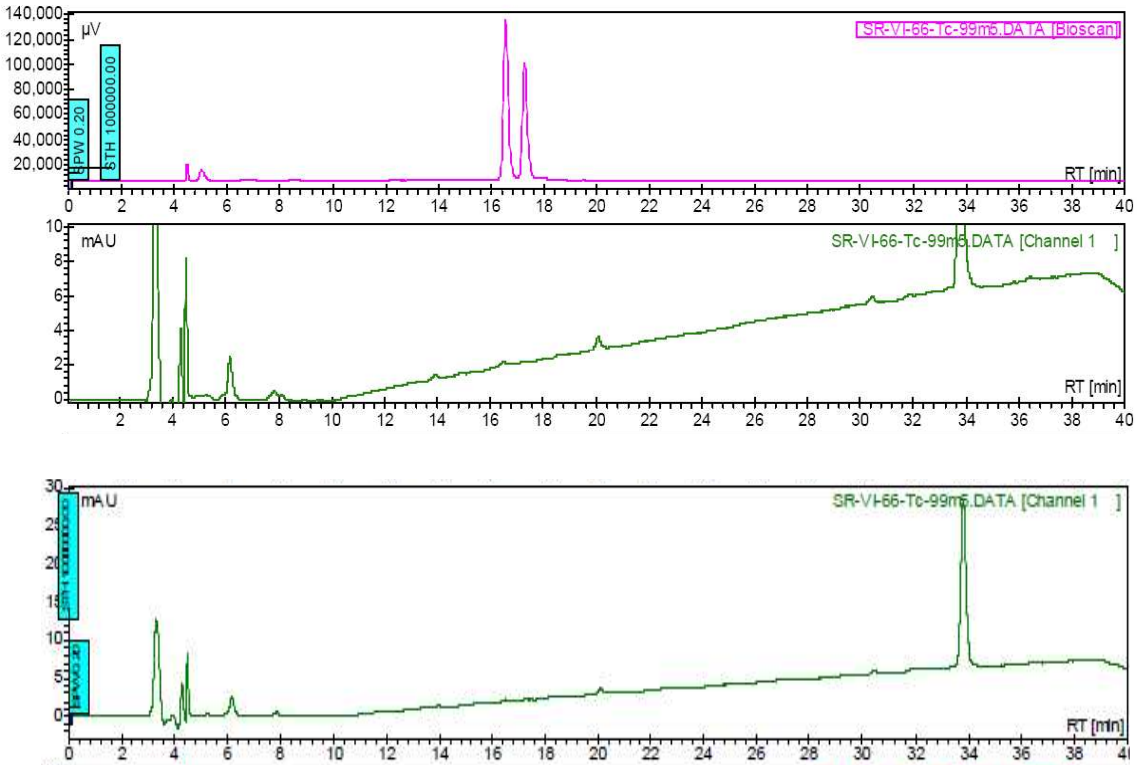


Preparative HPLC chromatograms for [$^{99m}$Tc]**L12**; radio-HPLC peak (top) uv peak at λ= 254nm (bottom) (HPLC Method 3). The uv peak at 29 min is unchelated **L12**

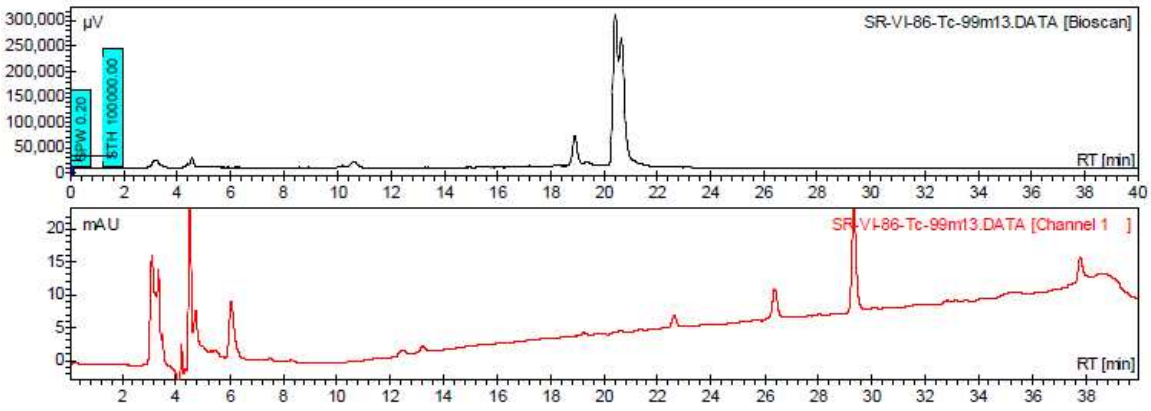

Preparative HPLC chromatograms for [$^{99m}$Tc]**L13**; radio-HPLC peak (top), uv peak at λ= 220 nm (middle) (HPLC Method 3). The uv peak at 31.6 min is unchelated **L13** shown at λ= 254 nm (bottom)

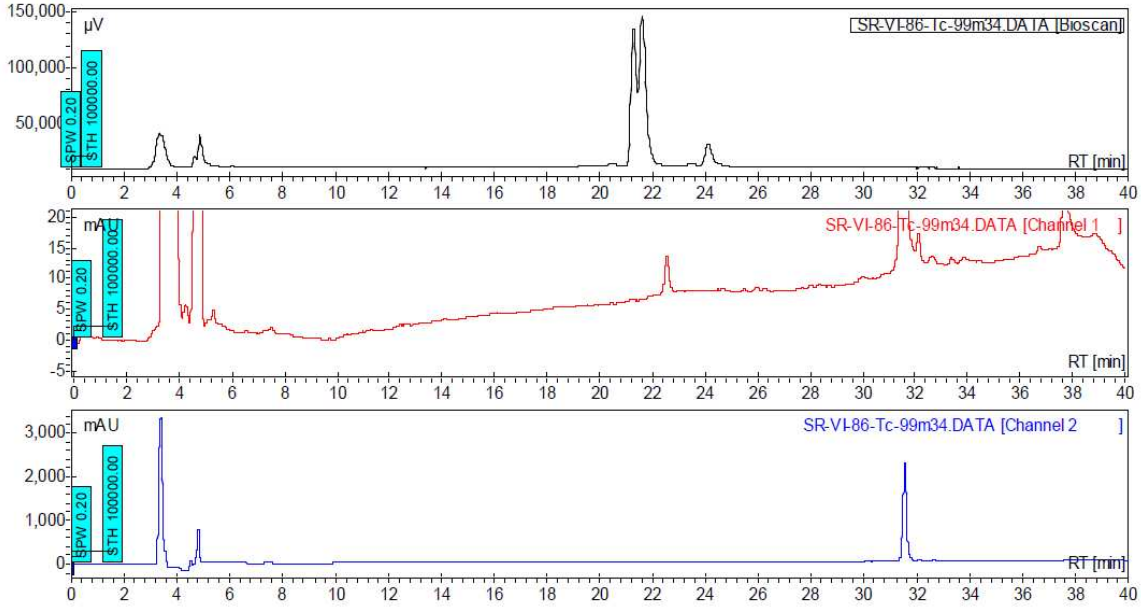


Preparative HPLC chromatograms for [$^{99m}$Tc]**L13**; radio-HPLC peak (top) uv peak at λ= 254nm (bottom) (HPLC Method 4) (inset: Expanded view from 0-20 min at λ= 254nm ). The uv peak at 33 min is unchelated **L13.**

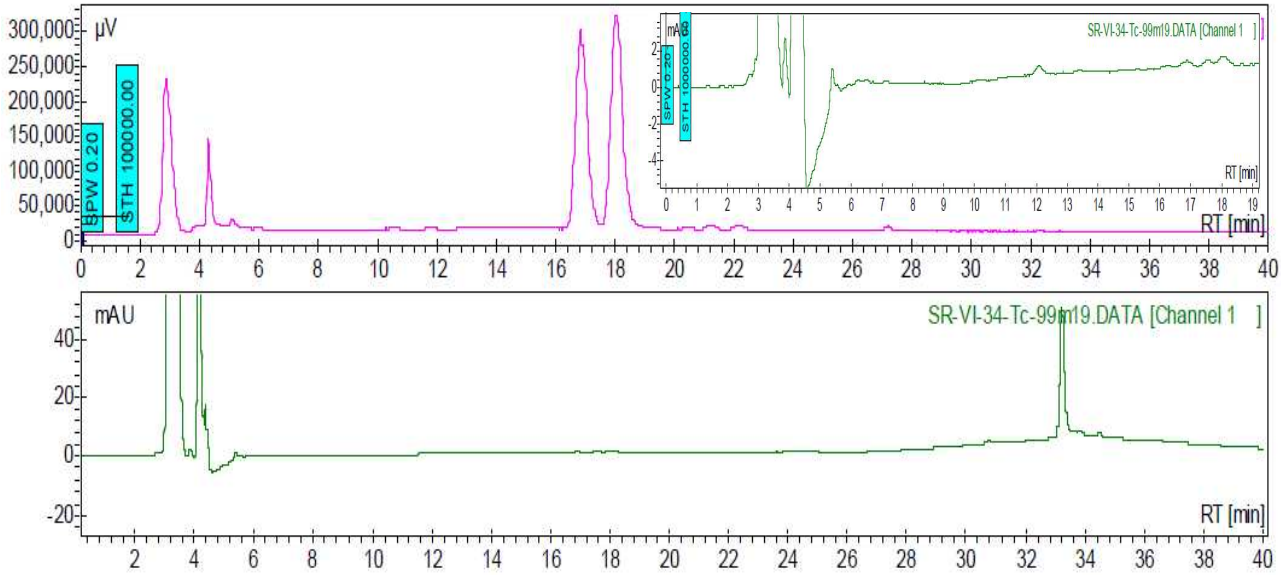

Preparative HPLC chromatograms for [$^{99m}$Tc]**L14**; radio-HPLC peak (top) (inset: expanded view of the chromatogram from 0-17 min at λ= 254nm), uv peak at λ= 254nm (bottom) (HPLC Method 3). (Inset)

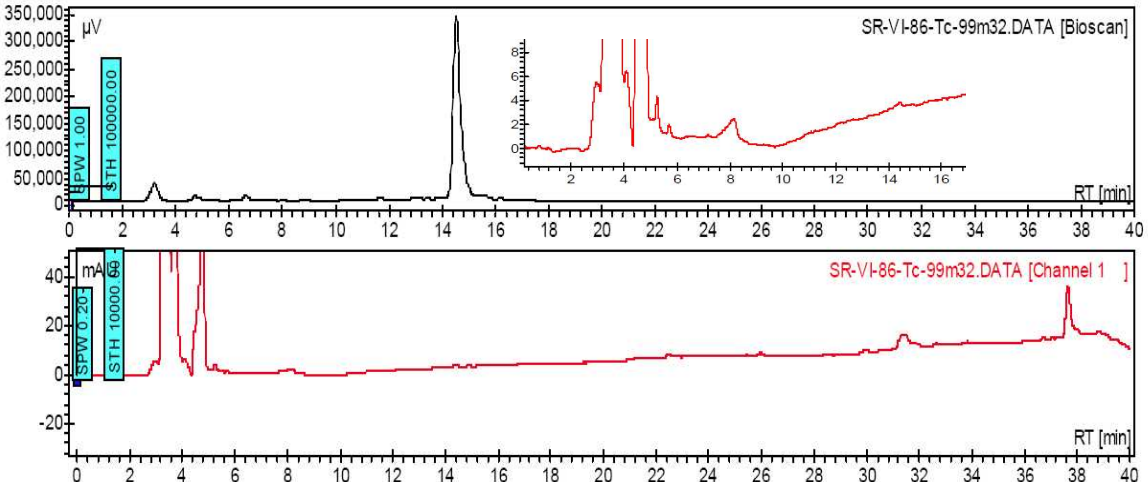


Preparative HPLC chromatograms for [$^{99m}$Tc]**L15**; radio-HPLC peak (top) uv peak at λ= 254nm (bottom) (HPLC Method 3). The uv peak at 25.3 min is unchelated **L15**.

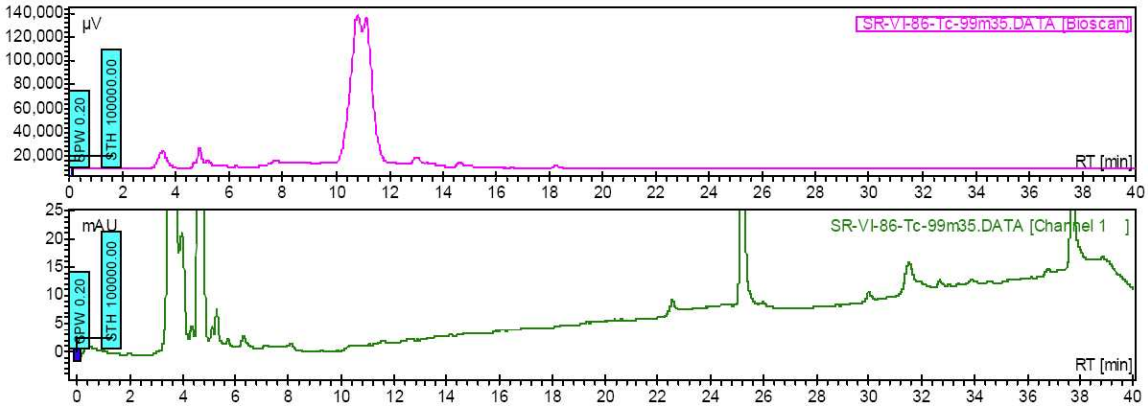

Stability study of [$^{99m}$Tc]**L15**. HPLC chromatograms for [$^{99m}$Tc]**L15** after 24 h incubation with 1X PBS solution at 25°C; radio-HPLC peak (top) uv peak at λ= 254nm (bottom) (HPLC Method 3).

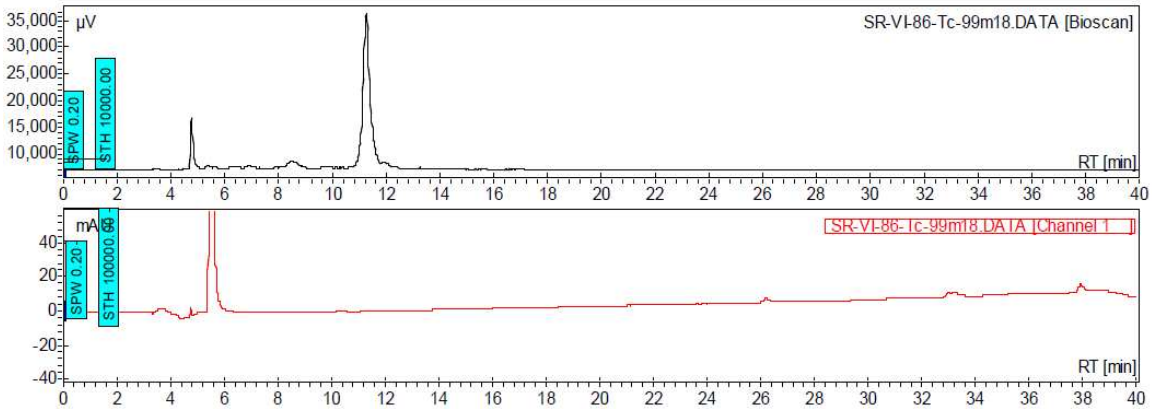


Preparative HPLC chromatograms for [$^{99m}$Tc]**L16**; radio-HPLC peak (top) uv peak at λ= 254nm (bottom) (HPLC Method 3).

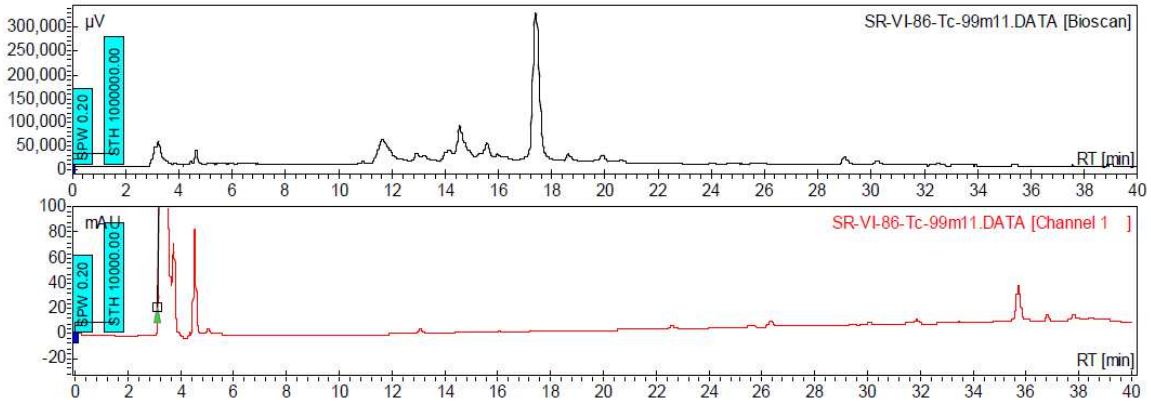

Preparative HPLC chromatograms for [$^{99m}$Tc]**L17**; radio-HPLC peak (top) uv peak at λ= 254 nm (bottom) (HPLC Method 3). (Inset: expanded view of the chromatogram from 0-16 min at λ= 254 nm)

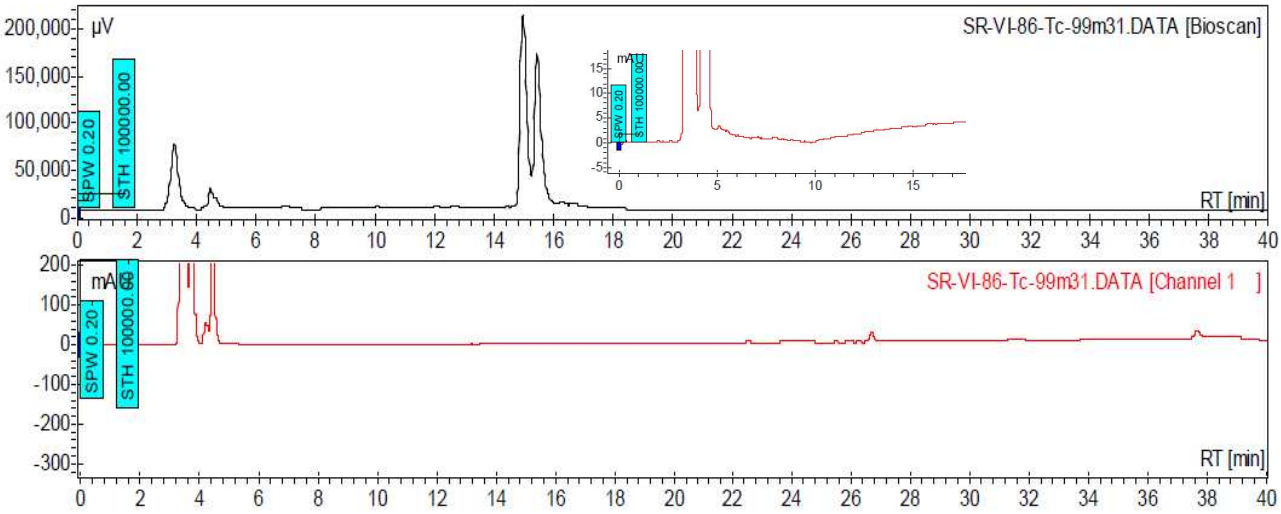

Preparative HPLC chromatograms for [$^{99m}$Tc]**L18**; radio-HPLC peak (top) uv peak at λ= 254 nm (bottom) (HPLC Method 3). (Inset: expanded view of the chromatogram from 0-16 min at λ= 254 nm)

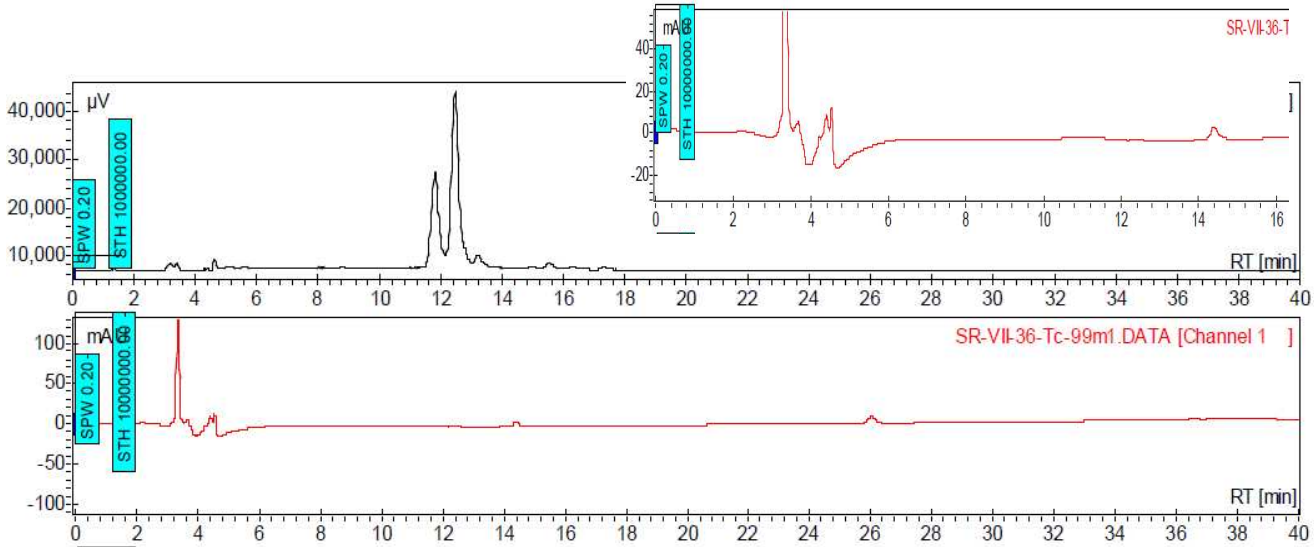


Preparative HPLC chromatograms for [$^{99m}$Tc]**L19**; radio-HPLC peak (top) uv peak at λ= 254 nm (bottom) (HPLC Method 5). The uv peak at 8.0 min is for the unchelated **L19**

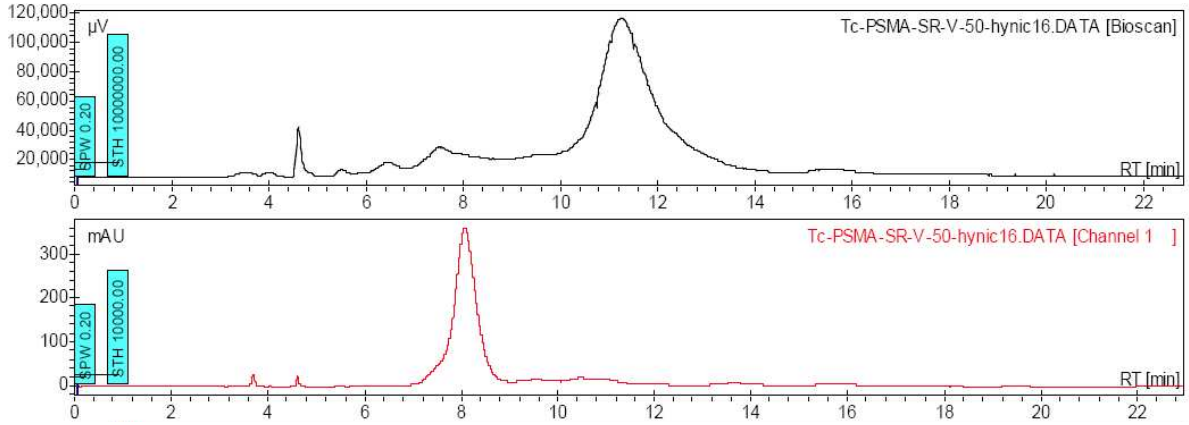

# Supporting Figures

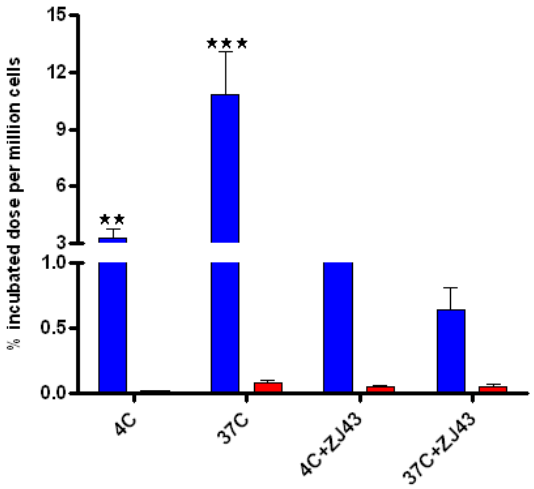


**Figure S1.** Uptake analysis of [$^{99m}$Tc]**L8** in PC3 PSMA+ PIP (blue) and PC3 PSMA- flu (red) cell lines at 4°C and 37°C. The radioactivity uptake in PIP cells was blocked by 10μmol ZJ43. Unpaired *t*-test used to analyze means of unblock vs block. *P*-value at 4°C was 0.0027- ** *P* value at 37°C was 0.0001- ***

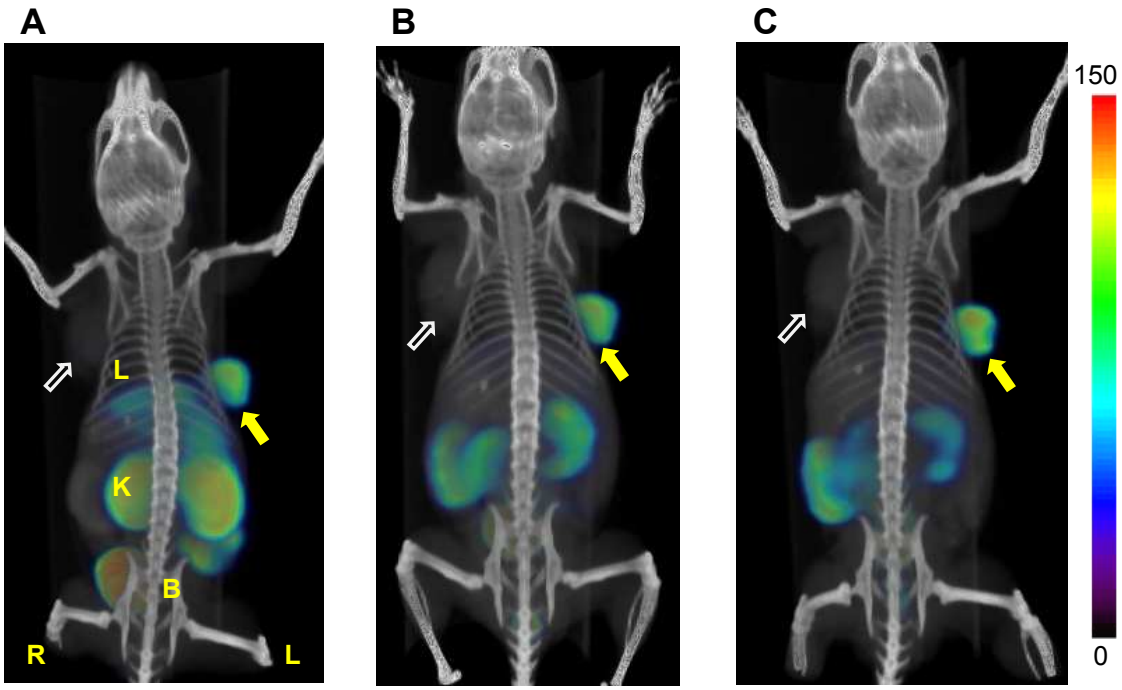


**Figure S2.** Small animal SPECT-CT imaging of PC3 PIP and PC3 flu tumor bearing mice with [$^{99m}$Tc]**L8** at 0.5 h (A), 2h (B), 6h (C) post injection of the tracer. PIP = PC3 PSMA+ PIP (solid arrow); flu = PC3 PSMA- flu (unfilled arrow); K= kidney; B = bladder; L = left; R = right. All images are decay-corrected and adjusted to the same maximum scale.

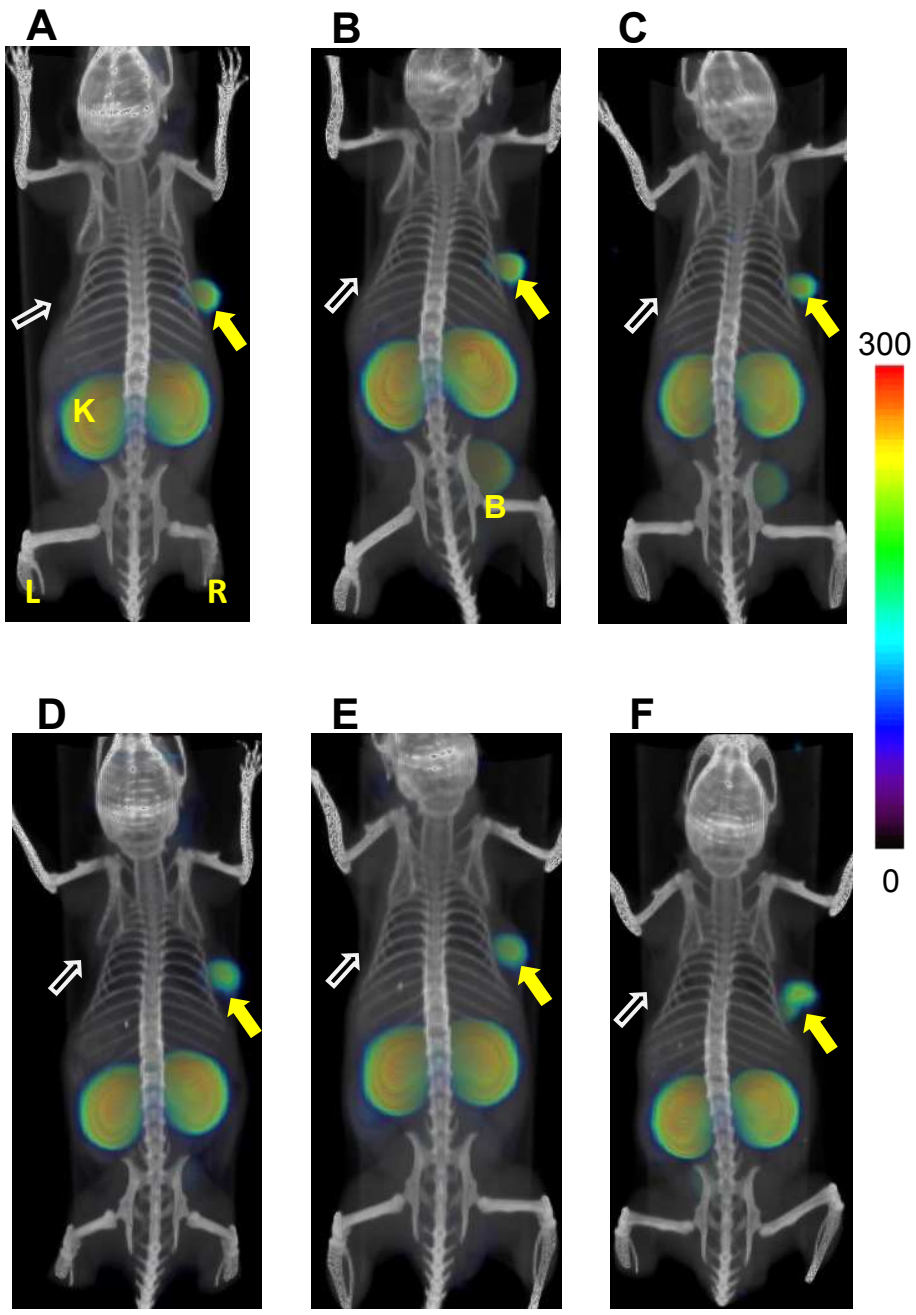


**Figure S3.** Whole body SPECT-CT imaging of PC3 PIP and PC3 flu tumor bearing mice with [$^{99m}$Tc]**L11A** (top) at 2 h (A), 6h (B), 18 h (C) and [$^{99m}$Tc]L11B (bottom) at 2 h (D), 6h (E), 18 h (F). PIP = PC3 PSMA+ PIP (solid arrow); flu = PC3 PSMA- flu (unfilled arrow); K= kidney; B = bladder; L = left; R = right. All images are decay-corrected and adjusted to the same maximum scale.

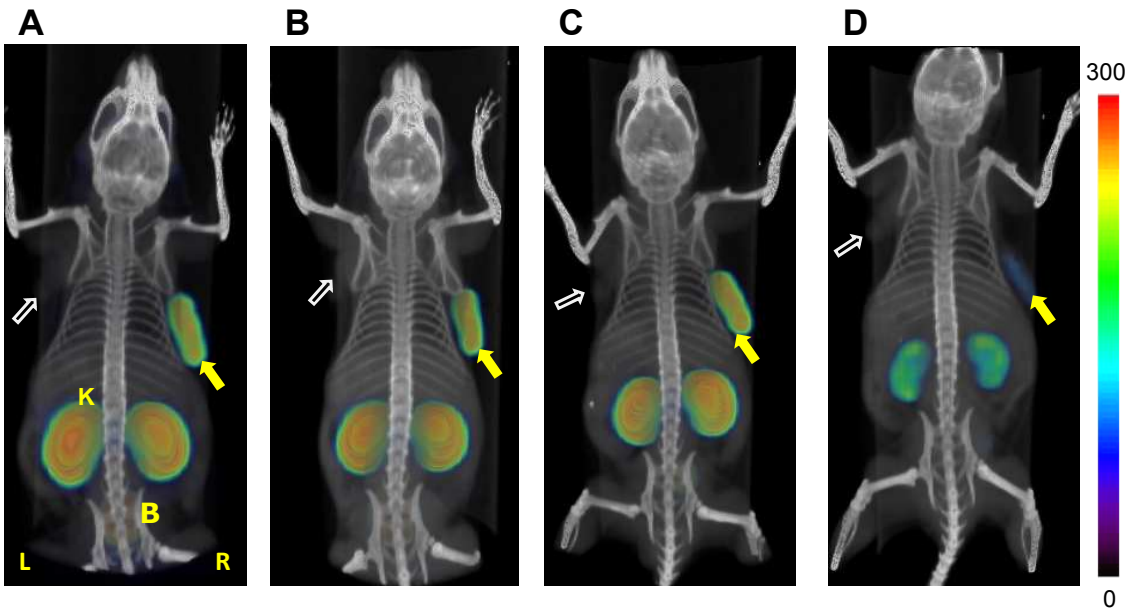


**Figure S4.** Small animal SPECT-CT imaging of PC3 PIP and PC3 flu tumor bearing mice with [$^{99m}$Tc]**L15** at 0.5 h (A), 2 h (B), 6h (C), 18 h (D). Abdominal radioactivity is primarily due to uptake within liver, spleen and kidneys and bladder. PIP = PC3 PSMA+ PIP (solid arrow); flu = PC3 PSMA- flu (unfilled arrow); K= kidney; L = left; R = right, B = bladder. All images are decay-corrected and adjusted to the same maximum scale.

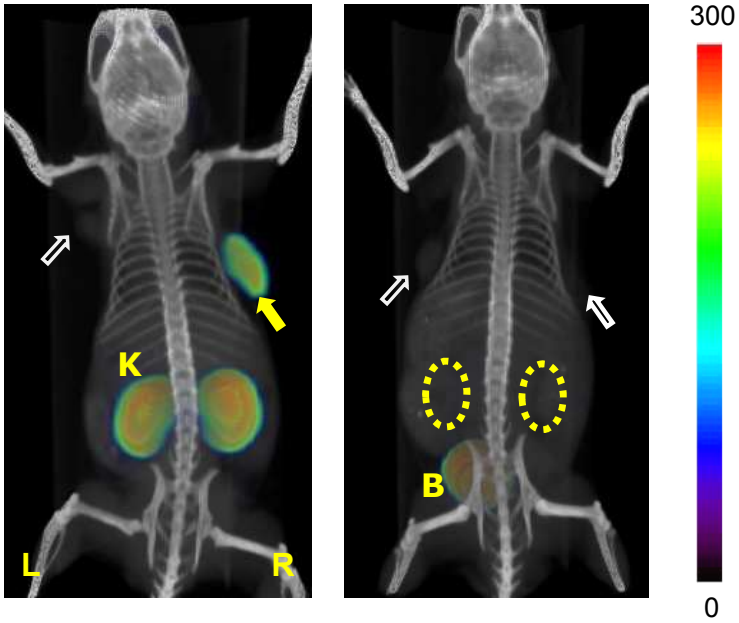


**Figure S5.** SPECT-CT imaging of PC3 PIP and PC3 flu tumor bearing mice of [$^{99m}$Tc]**L11** with (B) or without (A) the potent, selective PSMA inhibitor, ZJ-43, as the blocking agent administered 0.5 h before the radiotracer injection. Lack of radiopharmaceutical in both the tumor and kidneys (another PSMA+ site) upon co-treatment with ZJ-43 provides a further check on PSMA-specific binding. Images were acquired at 2h post injection.; K = kidney, L = left; R = right, B = bladder. All images are decay-corrected and adjusted to the same maximum scale.

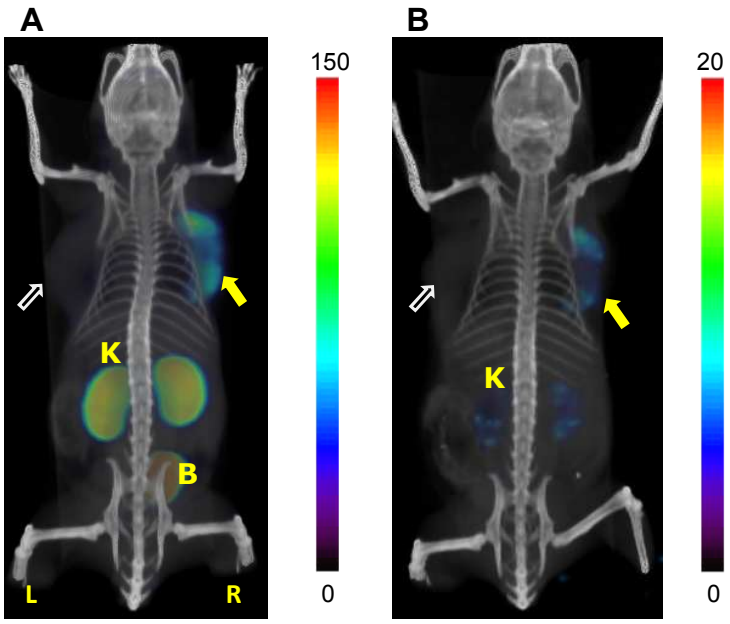


**Figure S6.** SPECT-CT imaging of PC3 PIP and PC3 flu tumor bearing mice with [$^{99m}$Tc]**L18** at 2 h (A), and 24 h (B). PIP = PC3 PSMA+ PIP (solid arrow); flu = PC3 PSMA- flu (unfilled arrow); K= kidney; B = bladder; L = left; R = right. All images are decay-corrected and adjusted to the same maximum scale.

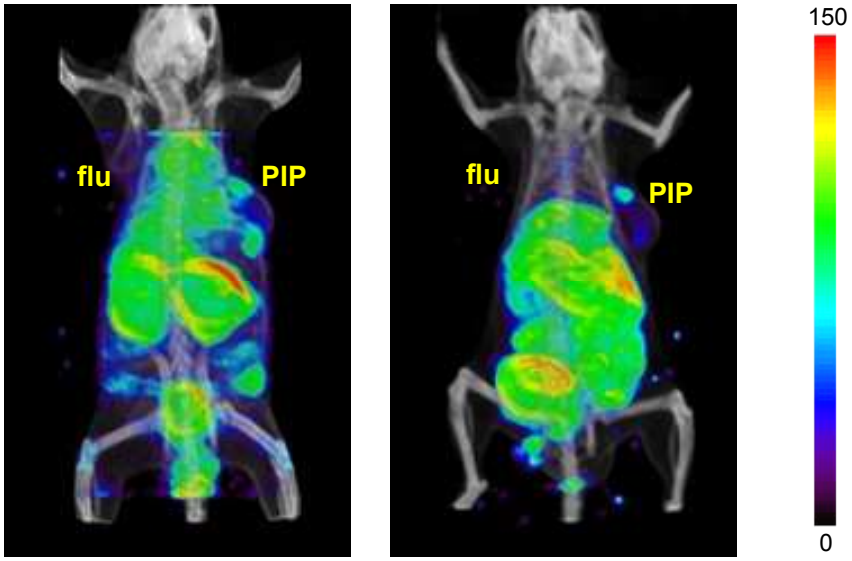


**Figure S7.** Whole body SPECT-CT imaging of PC3 PIP and PC3 flu tumor bearing mice with [$^{99m}$Tc]**L19** at 0.5h **(A)** and 3.5 h **(B).** PIP = PC3 PSMA+ PIP (solid arrow); flu = PC3 PSMA- flu (unfilled arrow) All images are decay-corrected and adjusted to the same maximum scale.

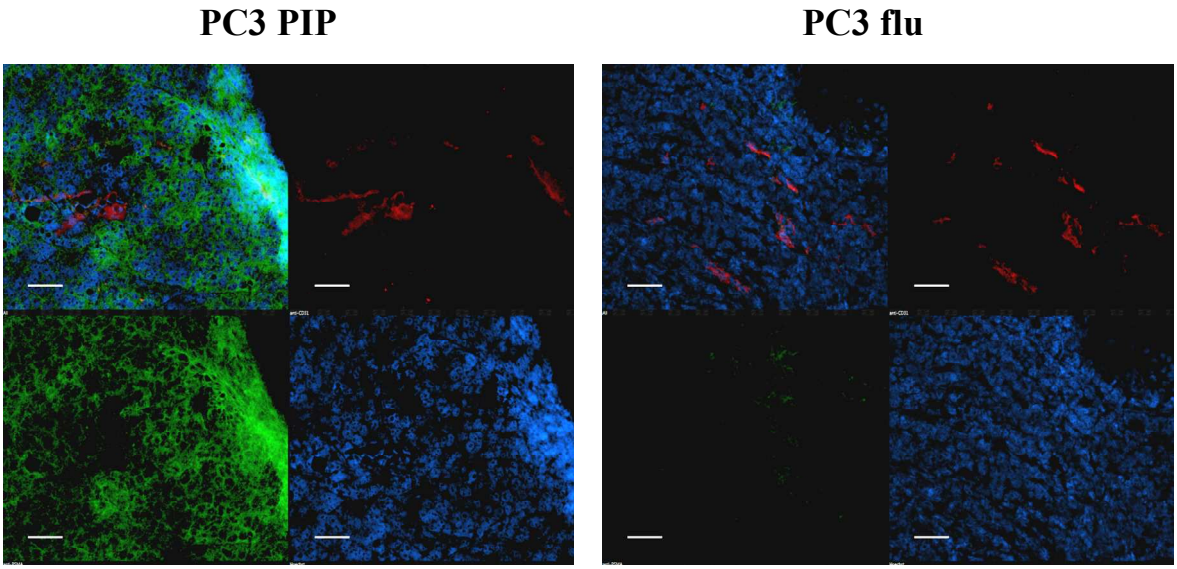


**Figure S8**. Epifluorescence micrographs of PC-3 PIP and PC-3 flu xenograft sections. Xenografts were cryosectioned to 20 micron thickness prior to staining with the following probes: Red: anti-CD31 Ab (vasculature); green: GCP05 anti-PSMA Ab; blue: Hoechst 33342; scale bar: 100 microns. Note lack of PSMA staining in the negative control cells (PC-3 flu).